ACS APPLIED MATERIALS & INTERFACES

Research Article

Cite This: ACS Appl. Mater. Interfaces 2018, 10, 33399−33406

www.acsami.org

Performance Improvement and Characterization of Spray-Coated Organic Photodetectors

Chia-Te Yen,[†] Yu-Ching Huang,*[,‡] Zheng-Lin Yu,[†] Hou-Chin Cha,[†] Hsia-Tsai Hsiao,[§] Yu-Ting Liang,[§] Forest Shih-Sen Chien,[∥] and Cheng-Si Tsao*[,†,⊥]

[†]Institute of Nuclear Energy Research, Longtan, Taoyaun 32546, Taiwan

[‡]Department of Materials Engineering, Ming Chi University of Technology, New Taipei City 24301, Taiwan

[§]AU Optronics Corporation, Hsinchu 30078, Taiwan

[∥]Department of Applied Physics, Tunghai University, Taichung 40704, Taiwan

[⊥]Department of Materials Science and Engineering, National Taiwan University, Taipei 10617, Taiwan

ABSTRACT: Low dark current organic photodetectors (OPDs) with a conventional structure consisting of poly(3-hexylthiophene) and [6,6]-phenyl-C_{61}-butyric acid methyl ester (PCBM) as active layer have been fabricated by spray-coating. Tuning the thickness of active layer and thermal annealing process for the spray-coated OPDs results in a remarkable performance with a low dark current density (J_d) of 2.90 × 10^{-8} A/cm^2 at reverse bias of 1 V. The impact of thermal annealing on the performance of sprayed OPDs is also investigated by the impedance analysis for mechanistic understanding. Our results demonstrate that the optimization of PCBM cluster and interfacial contact between the active layer and the metal electrode tailored by thermal annealing, respectively, could effectively reduce the J_d and increase the sensitivity of sprayed OPDs. The control of PCBM cluster is more important than the interfacial contact between the layers for improving J_d. In addition, structural characterization of the active layer studied by synchrotron small-angle X-ray scattering technique reveals why the spray-coated process can achieve the lowest dark current due to the favorable structure.

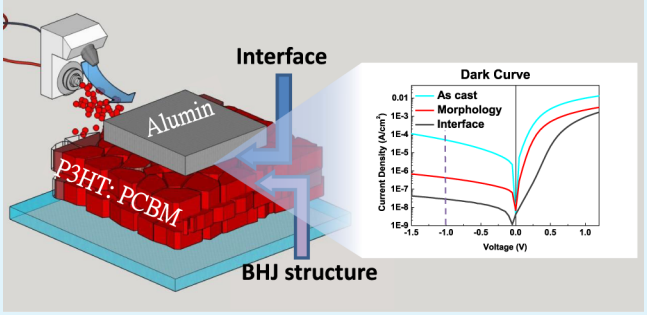

KEYWORDS: *organic photodetector, dark current, thermal anneal, BHJ structure, interface, impedance spectrum*

INTRODUCTION

Photodetectors have been broadly utilized in many applications, including image sensing, telecommunication, and security system. Organic photodetectors (OPDs) have attracted tremendous attention due to its low manufacturing cost, lightweight, and mechanical flexibility as compared to inorganic photodetectors.[1−4] Moreover, OPDs exhibit an effective light absorption spectrum from ultraviolet to near-infrared region, indicating that the OPDs perform a good photogeneration yield and sensitivity. The effective network structure in the active layer for OPDs is obtained by a blend of donor and acceptor materials and the subsequent treatments to from phase separation. The phase-separated bicontinuous network structure is called bulk heterojunction (BHJ) structure.[5−7] The BHJ structure has been widely adopted in organic electronics, such as organic photovoltaics (OPVs)[8−11] and OPDs.[12−15] Many studies have reported that the BHJ structure can not only increase the interfacial contact area between donor and acceptor materials for enhancing the separation of charge carriers but also facilitate the transport of charge carriers to the respective electrodes, thus enhancing the performance of the organic electronics.[16−19] The BHJ structure of the active layer can be tailored by various treatments.[20−22]

On the other hand, the large-area solution-processed printable techniques for organic electronics are suitable for the mass production processes, such as spray-coating[23−28] and slot-die coating.[29−32] The spray-coating process has emerged as a fast high-volume production technique to manufacture organic electronics. Moreover, the spray-coating process allows to easily control the thickness of the spray-coated film and to define the device pattern of the sprayed area by a mask. These features are very important to the commercialization and application of high-performance organic electronics. Although the feasibility of spray-coating process has been broadly investigated for OPVs,[23−26] there has been relatively little research in OPDs.[27,28]

The working principle of OPDs is similar to those of OPVs. However, the performance of OPVs mainly focuses on the improvement in short-circuit current and fill factor without any external reverse bias. The performance of OPDs emphasizes the achievement of low J_d and high photocurrent under reverse bias condition. Therefore, the performance requirements and

Received: September 1, 2018
Accepted: September 10, 2018
Published: September 10, 2018

Downloaded via SYNCHROTRON RADIATION RESEARCH on January 15, 2019 at 05:23:37 (UTC).
See https://pubs.acs.org/sharingguidelines for options on how to legitimately share published articles.

© 2018 American Chemical Society

DOI: 10.1021/acsami.8b15140
ACS Appl. Mater. Interfaces 2018, 10, 33399−33406

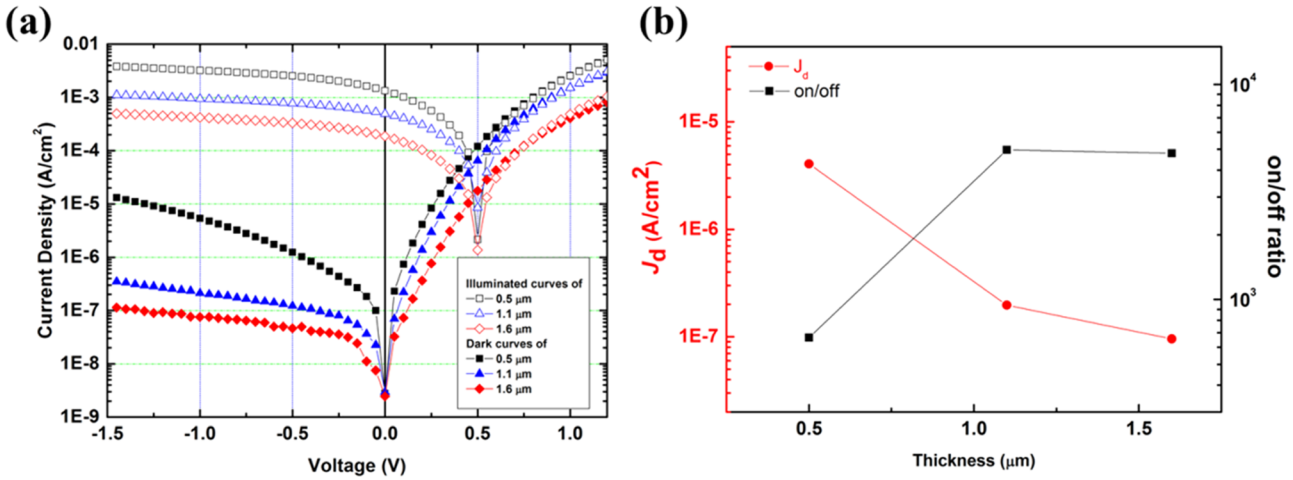

Figure 1. (a) J–V curves of OPDs with different active layer thicknesses under illumination and dark. (b) Corresponding J_d (at −1 V) and on/off ratio of these OPDs as a function of thickness.

research challenges of OPVs and OPDs are totally different, requiring new information and sufficient insights into how to design and fabricate highly efficient OPDs. Previous literature has reported that J_d and photocurrent are strongly influenced by the BHJ nanostructure of the active layer and the interfacial interaction between the adjacent layers of the devices.[33−35] How to optimize the nanostructure and interfacial interaction is substantially critical to the performance of OPDs. Thermal annealing has been widely used to effectively tailor the phase-separated bicontinuous (interpenetration) morphology of the active layer and thus enhance the efficiency of OPVs with a favorable BHJ structure.[36,37] Previous studies have also reported that the interfacial contact between the active layer and the metal electrode can be improved via thermal annealing.[38] Most studies focus on how to improve the interfacial contact between spray-coated active layer and substrate or top electrode by inserting a buffer layer,[27] adding solvent additives[39] or changing morphology.[40] All these studies put a lot of efforts in lowering the roughness to improve the interfacial contact. However, the insight into the commonly used thermal annealing effect on the dark current in OPDs use is neglected.

To promote the OPD resolution in light intensity sensing, increasing the on/off ratio between J_d and photocurrent is essential. Moreover, devices with lower J_d can detect weaker light sources. Several studies have suggested that the most effective ways to lower J_d of the OPDs is to insert an extra interfacial layer[41−44] or to increase the thickness of the active layer.[28,31,45−47] The commonly used approach is to raise the thickness of the active layer to achieve a high shunt resistance. However, there is often a trade-off between high photocurrent and low dark current of the OPDs due to the problem with charge recombination and space-charge effects in thick organic films.[48] Previous literature has addressed that the dark current and on/off ratio of the spray-coated OPDs are found to be of the order of $\sim 10^{-8}$ and $\sim 10^{3}$ A/cm^2, respectively.[27,28,49] The BHJ film thickness of these spray-coated OPDs was 500−800 nm, which was much thicker than that of the spin-coated OPDs (~300 nm). However, the spray-coated thick films were usually treated with the same thermal annealing process as used for the thin films.[31,41] Previous studies have indicated that the OPV devices with a thick active layer require a different thermal annealing treatment to achieve the optimal phase separation and performance.[50,51] Nevertheless, a systematic investigation of the effect of thermal annealing conditions on the performance of the spray-coated OPDs is still lacking.

In this study, we sequentially spray-coated the hole transport layer (HTL), poly(3,4-ethylenedioxythiophene):poly(styrene sulfonate) (PEDOT:PSS), and the active layer consisting of a blend of poly(3-hexylthiophene) (P3HT) and [6,6]-phenyl-C_{61}-butyric acid methyl ester (PCBM) on indium tin oxide (ITO)/glass substrate. The top metal electrode of Al was deposited by thermal evaporation. Regarding the spray process, the optimum thickness is determined here through the systematic study. We demonstrate the effect of different thermal annealing conditions on J_d and photocurrent under reverse bias of 1 V in which the BHJ structure and interfacial contact between layers were tailored, respectively. We revisited the simple and original method, thermal-annealing process, to provide an insight into the favorable structure (consisting of PCBM clusters and interfacial contact between layers). The improvements in interfacial interaction investigated by impedance measurement and film BHJ structure investigated by synchrotron grazing-incidence small-angle X-ray scattering (GISAXS) study, respectively, are correlated to variations in the dark current of OPDs. The effective synchrotron GISAXS is adopted in OPD research for the first time. This present study provides an in-depth analysis and integrated understanding regarding to the relationship among interfacial interaction, BHJ structure, and optoelectric properties of OPDs manufactured by mass-production technique.

EXPERIMENTAL SECTION

For fabricating the OPD, a hole transport layer (HTL) of PEDOT:PSS (Clevios PVP AI 4083 from H.C. Starck) was spray-coated on cleaned ITO-coated glass substrates (EMI-ito 15 from Optical Filter Ltd.). The ITO-coated glass substrates were cleaned by sonication in acetone and isopropanol (IPA) and treated with N_2 plasma for 3 min. The PEDOT:PSS was filtrated through a 0.45 μm filter and diluted with deionized water and IPA in the volume ratio of 2:1:7 (PEDOT:PSS/deionized water/IPA). The deposited HTL was dried in an ambient oven at 150 °C for 30 min. After drying, an o-xylene solution of P3HT and PCBM (Rieke Metals) in a weight ratio of 1:1 was spray-coated on the HTL. After that, a 1,2-dichlorobenzene overlayer was sprayed onto the P3HT/PCBM layer to modify the film into dense films.[20,21,23,52] In addition, the thickness of the P3HT/PCBM layer could be easily controlled by repeating the spraying

DOI: 10.1021/acsami.8b15140
ACS Appl. Mater. Interfaces 2018, 10, 33399−33406

cycle. An aluminum electrode (100 nm) was thermally deposited on the active layer through a shadow mask of 0.3 cm^2 afterward. A systematic comparison of devices before and after annealing was performed to clarify the effect of morphological change and interfacial contact between the active layer and the electrode on the OPD performance. The active layers have been thermally annealed before cathode deposition at various temperatures for 10 min in a N_2-filled glovebox, which is termed as preannealed devices. The devices thermally annealed after the cathode deposition are named postannealed devices. In addition, we also prepared some devices without annealing as reference devices. Current−voltage curves were recorded using Keithley 2400 Source Meter in dark and under 100 mW/cm^2 simulated AM 1.5G irradiation (Abet technologies, model #11000). The thickness of the active layer was measured by using a KLA Tencor Alpha-Step D-100 stylus profiler. The impedance spectra were measured using Zahner IM6. The impedance spectra were recorded in the frequency range from 2 MHz to 50 mHz with the potential amplitude of 50 mV.

RESULTS AND DISCUSSION

Many studies have reported that J_d is directly related to the thickness of the active layer.[27,28,31] To lower the dark current density (J_d) of the OPD, we first adjust the film thickness of the active layer by spray-coating the films in various spraying cycles. We deposited the films in 5, 10, and 15 spraying cycles for preparing the film thicknesses of 0.5, 1.1, and 1.6 μm, respectively. Figure 1 shows the dark current and photocurrent of the spray-coated films as a function of film thicknesses. Figure 1a shows that the dark current at −1 V decreases with increasing sprayed film thickness. The low dark current of 9.55×10^{-8} A/cm^2 was achieved for the sprayed film with the thickness of 1.6 μm. In addition, the photocurrent at −1 V also decreases with increase in the spray-coated film thickness. The on/off ratio is defined by J_d and photocurrent at −1 V. The relationship among the dark current, on/off ratio, and film thickness of the spray-coated devices is plotted in Figure 1b, and the photoelectric characteristics are listed in Table 1. J_d of the spray-coated OPD dramatically decreases in the order of 10^{-6} to 10^{-8} when the thickness of the active layer increases from 0.5 to 1.1 μm and J_d goes toward saturation over 1.1 μm. On the other hand, there is a trade-off between J_d and photocurrent. Figure 1a shows that the photocurrent decreases with the increasing thickness of the active layer. The reduction in photocurrent may be a result of the high resistance of the thick active layer. The on/off ratio improves initially with the increase in the thickness of the active layer from 0.5 to 1.1 μm, and the on/off ratio shows a saturation as the active layer thickness reaches 1.6 μm. Therefore, we fabricated the active layer based on the thickness of 1.6 μm to investigate the other treatment effects for improving both dark current and on/off ratio. According to our previous results,[7,23,53,54] thermal annealing is critical for the performance of spray-coated OPVs. Because the thickness of the active layer of the spray-coated OPD here is much thicker than that of the sprayed OPV (~300 nm), we have to optimize the thermal annealing condition of the spray-coated OPDs to improve performance. First, we postannealed (annealing after Al deposition) these devices for 10 min at different annealing temperatures of 110, 145, and 180 °C. The $J-V$ characterization of these devices is shown in Figure 2a and listed in Table 2. The J_d at −1 V decreases from 1.35×10^{-6} to 3.87×10^{-8} A/cm^2 as the annealing temperature increases from 110 to 180 °C. In addition, the corresponding photocurrent is also enhanced from 3×10^{-3} to 1×10^{-2} A/cm^2 by increasing the annealing temperature. Figure 2b shows the effect of postannealing temperature on the J_d and on/off ratio of the spray-coated OPD. A sharp drop (~1 order) in J_d appears when the postannealing temperature is increased from 110 to 145 °C. However, J_d showed a slow decay (much less 1 order) with further increase in the annealing temperature up to 180 °C. The trend clearly demonstrates that the significant change in J_d occurred over annealing temperature of 110 °C in which 110 °C is close to the glass-transition temperature (T_g) of P3HT.[45,55] Generally, the postannealing process involves not only the BHJ structure of the active layer but also the interfacial contact between the active layer and the metal electrode. Therefore, the low J_d and improved on/off ratio may have resulted from (1) the favorable BHJ structure formed by the phase separation between P3HT and PCBM regarding the spray process and layer thickness (different from that of OPV device) and (2) the good interfacial contact between the active layer and Al improved by the thermal effect of postannealing.[56,57]

Table 1. Dark Current Density and on/off Ratio of Spray-Coated OPDs with Different Active Layer Thicknesses under Reverse Bias of 1 V

thickness (μm)	J_d (A/cm^2)	on/off ratio
0.5	4.06×10^{-6}	6.65×10^2
1.1	1.97×10^{-7}	4.97×10^3
1.6	9.55×10^{-8}	4.79×10^3

To further clarify the contributions of the BHJ structure and the interfacial contact between layers to the performance improvement, we preannealed (annealing before Al deposition) the spray-coated OPDs at 180 °C for 10 min and evaluated the performance of OPDs. Compared to the postannealed OPD, the preannealed OPD device has the same improved BHJ structure of the active layer but has the raw interfacial contact. In addition, the nonannealing OPDs were also used as reference devices to clarify the effect of the preannealing process (i.e., BHJ structure) on the performance of spray-coated OPDs. Figure 3 shows the variation in the $J-V$ curves of OPDs with various annealing processes and Table 3 summarizes the performance of OPDs for facilitating us to understand the impact of annealing process on the active layer. The spray-coated OPDs with preannealing show an improvement with a much lower J_d (4.23×10^{-7} A/cm^2) as compared to the sprayed OPDs without annealing (5.23×10^{-5} A/cm^2), indicating the effect of thermally enhanced BHJ structure on the dark current. However, the photocurrents for both preannealed and nonannealed OPDs are similar. Thus, the on/off ratios of these OPDs mainly depend on the J_d of these devices. Noteworthy is that the spray-coated active layer upon annealing process can improve the leakage current of the sprayed OPDs by 2 orders of magnitude. Moreover, the spray-coated OPDs with postannealing exhibit further improvement in the averaged values of J_d and the on/off ratio of 2.90×10^{-8} A/cm^2 and 2.90×10^4, respectively. The postannealing process improves not only the BHJ structure of the spray-coated active layer but also the interfacial contact between the active layer and the metal electrode. Further reduction in J_d from 4.23×10^{-7} to 2.90×10^{-8} A/cm^2 is attributed to better interfacial contact between the active layer and the metal electrode. On the basis of these results, we calculated the J_d ratio of the spray-coated OPDs with different annealing treatments to show the impact of annealing process on the dark current of sprayed

DOI: 10.1021/acsami.8b15140
ACS Appl. Mater. Interfaces 2018, 10, 33399−33406

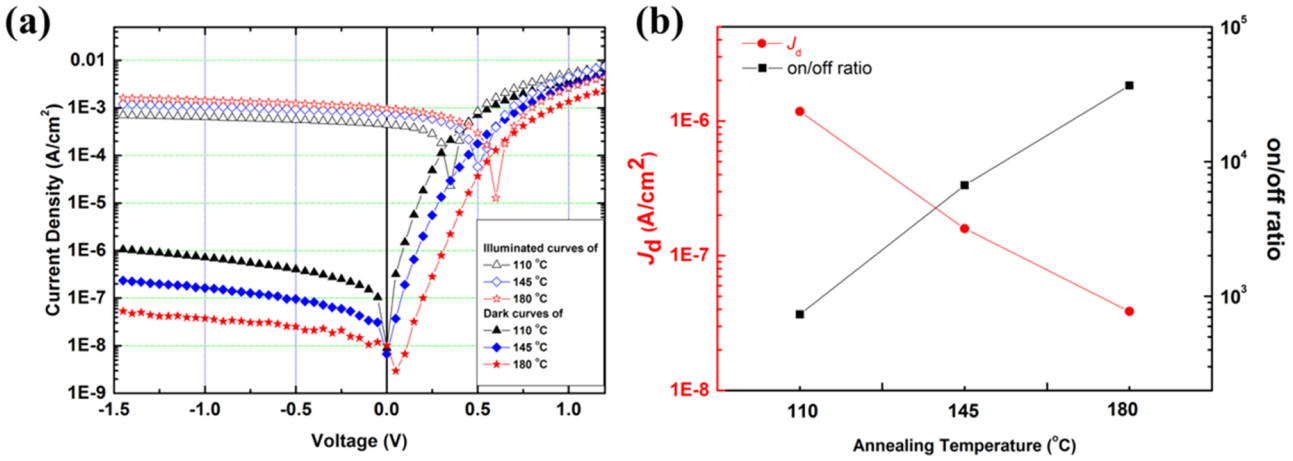

Figure 2. (a) J–V curves of OPDs prepared at different postannealing temperatures under illumination and dark. (b) Corresponding J_d (at −1 V) and on/off ratio of these OPDs as a function of annealing temperature.

Table 2. Dark Current Density and on/off Ratio of Spray-Coated OPDs with Different Postannealing Temperatures under Reverse Bias of 1 V

annealing temp. (°C)	J_d (A/cm^2)	on/off ratio
110	1.18×10^{-6}	7.33×10^{2}
145	1.60×10^{-7}	6.69×10^{3}
180	3.87×10^{-8}	3.67×10^{4}

Table 3. Dark Current Density and on/off Ratio of Spray-Coated OPDs with Different Thermal Annealing Processes under Reverse Bias of 1 V

anneal process	J_d (A/cm^2)	on/off ratio
none	5.23×10^{-5}	4.59
pre	4.23×10^{-7}	6.95×10^{2}
post	2.90×10^{-8}	2.90×10^{4}

OPD. We define the J_d ratio of nonannealed OPDs to preannealed OPDs as R_{np}, and the J_d ratio of preannealed OPDs to postannealed OPDs as R_{pp}. The R_{np} and R_{pp} are mainly related to the effect of BHJ structure and the interfacial contact between the active layer and the metal electrode on J_d, respectively. According to Table 3, the calculated R_{np} value (=123) is higher than the R_{pp} value (=14). These data indicate that compared to the reduction in J_d due to the improvement in the good interfacial contact, the main reduction in J_d is controlled by the BHJ structure. Furthermore, we employ impedance measurement to demonstrate how the annealing process has a strong influence on the behavior of charge transport and recombination in the sprayed OPDs.

The impedance spectra of the spray-coated OPDs were carried out under 0 V bias in dark. Figure 4a,b show the Nyquist plots and the imaginary impedance spectra, respectively. The Nyquist plots comprise two semicircles. The inset in Figure 4a shows small semicircles near the origin at high frequency. The carrier dynamics of the diffusion–recombination processes in the devices can be represented by the equivalent model of the series of two parallel resistor and constant phase element (CPE) circuits, as shown in Figure 4c.[58] In this model, R_s represents the effective series resistance of bulk materials and ohmic contacts. R_{ct} and CPE_{ct} represent the semicircle at high frequency associated with the charge transit at the active layer/electrode interfaces. R_{rec} and CPE_{rec} represent the semicircle at low frequency associated with the exciton recombination in the active layer. The impedance of a CPE can be rewritten as

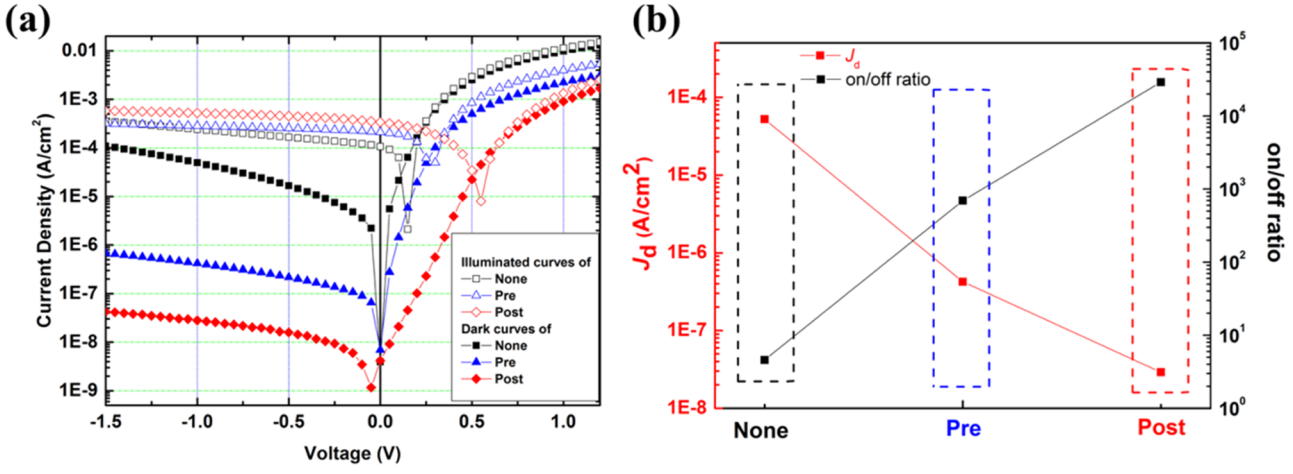

Figure 3. (a) J–V curves of OPDs with different thermal annealing processes under illumination and dark. (b) Comparison of J_d (at −1 V) and on/off ratios corresponding to these OPDs.

DOI: 10.1021/acsami.8b15140
ACS Appl. Mater. Interfaces 2018, 10, 33399–33406

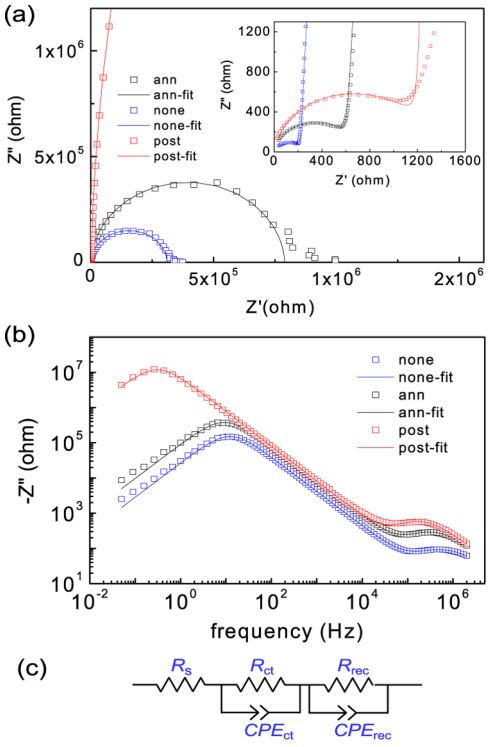

Figure 4. (a) Representative impedance spectra of spray-coated OPDs with various thermal annealing treatments including none, pre-, and postannealing processes. The inset highlights the impedance spectra at high frequency. (b) Imaginary component of the impedance (Z'') versus log$f$. (c) Equivalent circuit of spray-coated OPDs.

$$Z_{\mathrm{CPE}} = \frac{1}{B(i\omega)^{P}} \tag{1}$$

where B and P constants are the frequency-independent magnitude and phase parameters, respectively.[59] The charge transit rate (f_{ct}) at the active layer/electrode interface and the recombination rate (f_{rec}) in the active layer are exactly the characteristic frequencies of the Z'' peaks at high and low frequency, respectively. The characteristic frequency can also be obtained with the corresponding parameters, R, B, and P, by

$$f = \frac{1}{2\pi}\frac{1}{(R \times B)^{P}} \tag{2}$$

We fitted the impedance spectra according to the equivalent model by the ZView software to obtain the impedance parameters shown in Table 4. Both pre- and postannealing can cause a decrease in f_{rec}, evidenced by the calculated values in Table 4 and the shift of the peaks to lower frequency in the Bode plots of imaginary impedance. Especially, R_{rec} increases dramatically by a factor of 80 after postannealing and causes a significant decrease in f_{rec} by a factor of 40. Namely, charge recombination at the active layer is largely suppressed, which is consistent with the measurement of J_d reduction. It is worth noting that f_{ct} also decreases by a factor of 3 with annealing because of the increase in R_{ct} after annealing. However, the decreases in f_{ct} were minor as compared to the decrease in f_{rec}.

Furthermore, GISAXS is an effective tool to study the size and amount of nanoscale PCBM clusters in the BHJ structure of active layer according to the previous studies.[60−62] The photoelectric properties of the device are determined by the BHJ structure, such as the size, amount, and dispersion of PCBM clusters. Basically, the structural feature and role of nanoscale PCBM clusters closely related to the charge separation and transport of electron in the typical solar cells should be different from those of PCBM clusters in the photodetector operation. It is fundamentally interesting to explore the difference between the PCBM clusters formed in the thick spray-coated film and the well-used spin-coated film regarding the performance of low dark current. Figure 5 shows

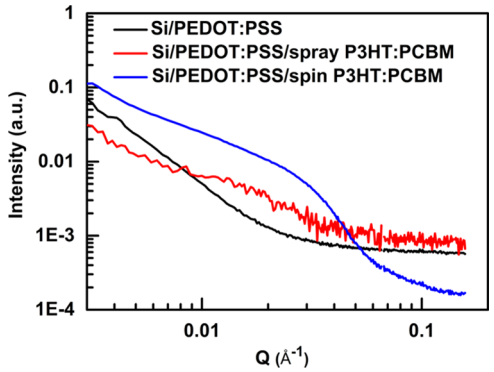

Figure 5. GISAXS profiles of the spray-coated P3HT/PCBM film with a thickness of ∼1 μm and the spin-coated P3HT/PCBM film.

the comparison of GISAXS profiles of the spray-coated and the spin-coated P3HT/PCBM films as the reference group. The shoulder peaks of the spray- and spin-coated film located at scattering vector Q = 0.017 and 0.025 Å^{-1} correspond to the cluster size of ∼20 and ∼6 nm, respectively.[62] Because the GISAXS peak intensities of both films (related to the volume fraction of clusters) show similar amplitude, it can be speculated that clusters in the spray-coated film have a much larger spacing between the clusters due to their relatively large cluster size compared to the small and dense clusters in the spin-coated film. This present study points out that the large PCBM clusters spacing inherently formed in the BHJ structure may play a critical role in suppressing the dark current. However, the PCBM cluster spacing is still controlled in the limited range to keep a certain benefit to electron transport in the BHJ structure of solar cell operation and thus have a good on/off ratio. The P3HT structure studied by the simultaneously grazing-incidence wide-angle scattering in this work does not show the significant correlation compared to the PCBM cluster.

Table 4. Values of Impedance Parameters of Sprayed OPDs with Different Thermal Annealing Processes in Dark

anneal process	R_s (Ω)	R_{ct} (Ω)	B_{ct} (nF)	P_{ct}	f_{ct} (kHz)	R_{rec} (kΩ)	B_{rec} (nF)	P_{rec}	f_{rec} (Hz)
non	3.10×10^{-6}	220	16.3	0.83	579	311	46.6	0.98	12.0
pre	8.26×10^{-7}	606	2.78	0.91	352	788	24.7	0.97	9.2
post	3.10×10^{-6}	1200	1.99	0.93	177	24 500	21.6	0.99	0.3

DOI: 10.1021/acsami.8b15140
ACS Appl. Mater. Interfaces 2018, 10, 33399−33406

CONCLUSIONS

We improve the performance of the spray-coated OPDs with remarkably low dark current at a reverse bias of 1 V by tuning the spray-coated film thickness of the active layer and thermal annealing process. The optimal OPDs prepared with the film thickness of 1.6 μm and postannealing exhibit a J_d of 2.90 × 10^{-8} A/cm^2 and a on/off ratio of 2.90 × 10^4. The J_d of the spray-coated OPDs could dramatically decrease when the OPDs are thermally annealed at temperature higher than the T_g of P3HT polymer. This result reveals that J_d was highly related to the phase-separated BHJ nanostructure of P3HT and PCBM. We also show the effect of the nanostructure and interfacial contact between the active layer and Al, respectively, on the performance of the sprayed OPDs treated under different annealing conditions. Our results demonstrate that the PCBM clusters play a more important role in the J_d reduction of the spray-coated OPDs than the interfacial contact between layers. Furthermore, our impedance analysis demonstrates that the spray-coated OPDs treated with postannealing exhibit the highest impedance. In addition, the shift in low and high frequency of the imaginary part of impedance to frequency shows that the postannealing device exhibits a relatively high sensitivity than other two devices.

AUTHOR INFORMATION

Corresponding Authors

*E-mail: huangyc@mail.mcut.edu.tw.
*E-mail: cstsao@iner.gov.tw.

ORCID

Yu-Ching Huang: 0000-0003-4772-8050

Notes

The authors declare no competing financial interest.

ACKNOWLEDGMENTS

The authors would like to acknowledge the financial support from the Ministry of Science and Technology of Taiwan (Grant No. 107-2218-E-131-007-MY3).

REFERENCES

(1) Yang, D. Z.; Zhou, X. K.; Ma, D. G. Fast Response Organic Photodetectors with High Detectivity Based on Rubrene And C60. *Org. Electron.* **2013**, *14*, 3019−3023.

(2) Binda, M.; Natali, D.; Iacchetti, A.; Sampietro, M. Integration of an Organic Photodetector onto a Plastic Optical Fiber by Means of Spray Coating Technique. *Adv. Mater.* **2013**, *25*, 4335−4339.

(3) Yang, D. Z.; Ma, D. G. 1,1-Bis[(di-4-tolylamino)phenyl]-cyclohexane for Fast Response Organic Photodetectors with High External Efficiency And Low Leakage Current. *J. Mater. Chem. C* **2013**, *1*, 2054−2060.

(4) Liu, Z. Y.; Parvez, K.; Li, R. J.; Dong, R. H.; Feng, X. L.; Mullen, K. Transparent Conductive Electrodes from Graphene/PEDOT:PSS Hybrid Inks for Ultrathin Organic Photodetectors. *Adv. Mater.* **2015**, *27*, 669−675.

(5) Liao, H. C.; Tsao, C. S.; Shao, Y. T.; Chang, S. Y.; Huang, Y. C.; Chuang, C. M.; Lin, T. H.; Chen, C. Y.; Su, C. J.; Jeng, U. S.; Chen, Y. F.; Su, W. F. Bi-Hierarchical Nanostructures of Donor-Acceptor Copolymer And Fullerene for High Efficient Bulk Heterojunction Solar Cells. *Energy Environ. Sci.* **2013**, *6*, 1938−1948.

(6) Huang, Y. C.; Tsao, C. S.; Chuang, C. M.; Lee, C. H.; Hsu, F. H.; Cha, H. C.; Chen, C. Y.; Lin, T. H.; Su, C. J.; Jeng, U. S.; Su, W. F. Small- and Wide-Angle X-ray Scattering Characterization of Bulk Heterojunction Polymer Solar Cells with Different Fullerene Derivatives. *J. Phys. Chem. C* **2012**, *116*, 10238−10244.

(7) Huang, Y. C.; Tsao, C. S.; Cha, H. C.; Chuang, C. M.; Su, C. J.; Jeng, U. S.; Chen, C. Y. Correlation between Hierarchical Structure and Processing Control of Large-area Spray-coated Polymer Solar Cells toward High Performance. *Sci. Rep.* **2016**, *6*, No. 20062.

(8) Liu, Y. H.; Zhao, J. B.; Li, Z. K.; Mu, C.; Ma, W.; Hu, H. W.; Jiang, K.; Lin, H. R.; Ade, H.; Yan, H. Aggregation and Morphology Control Enables Multiple Cases of High-Efficiency Polymer Solar Cells. *Nat. Commun.* **2014**, *5*, No. 5293.

(9) Zhou, H.; Zhang, Y.; Seifter, J.; Collins, S. D.; Luo, C.; Bazan, G. C.; Nguyen, T. Q.; Heeger, A. J. High-Efficiency Polymer Solar Cells Enhanced by Solvent Treatment. *Adv. Mater.* **2013**, *25*, 1646−1652.

(10) Liao, S. H.; Jhuo, H. J.; Yeh, P. N.; Cheng, Y. S.; Li, Y. L.; Lee, Y. H.; Sharma, S.; Chen, S. A. Single Junction Inverted Polymer Solar Cell Reaching Power Conversion Efficiency 10.31% by Employing Dual-Doped Zinc Oxide Nano-Film as Cathode Interlayer. *Sci. Rep.* **2014**, *4*, No. 6813.

(11) He, Z. C.; Xiao, B.; Liu, F.; Wu, H. B.; Yang, Y. L.; Xiao, S.; Wang, C.; Russell, T. P.; Cao, Y. Single-Junction Polymer Solar Cells with High Efficiency And Photovoltage. *Nat. Photonics* **2015**, *9*, 174−179.

(12) Dong, R.; Bi, C.; Dong, Q. F.; Guo, F. W.; Yuan, Y. B.; Fang, Y. J.; Xiao, Z. G.; Huang, J. S. An Ultraviolet-to-NIR Broad Spectral Nanocomposite Photodetector with Gain. *Adv. Opt. Mater.* **2014**, *2*, 549−554.

(13) Zhou, X. K.; Yang, D. Z.; Ma, D. G. Extremely Low Dark Current, High Responsivity, All-Polymer Photodetectors with Spectral Response from 300 nm to 1000 nm. *Adv. Opt. Mater.* **2015**, *3*, 1570−1576.

(14) Qi, J.; Zhou, X. K.; Yang, D. Z.; Qiao, W. Q.; Ma, D. G.; Wang, Z. Y. Optimization of Solubility, Film Morphology and Photodetector Performance by Molecular Side-Chain Engineering of Low-Bandgap Thienothiadiazole-Based Polymers. *Adv. Funct. Mater.* **2014**, *24*, 7605−7612.

(15) Zhang, L.; Yang, T. B.; Shen, L.; Fang, Y. J.; Dang, L.; Zhou, N. J.; Guo, X. G.; Hong, Z. R.; Yang, Y.; Wu, H. B.; Huang, J. S.; Liang, Y. Y. Toward Highly Sensitive Polymer Photodetectors by Molecular Engineering. *Adv. Mater.* **2015**, *27*, 6496−6503.

(16) Scharber, M. C.; Sariciftci, N. S. Efficiency of Bulk-Heterojunction Organic Solar Cells. *Prog. Polym. Sci.* **2013**, *38*, 1929−1940.

(17) Peumans, P.; Uchida, S.; Forrest, S. R. Efficient Bulk Heterojunction Photovoltaic Cells Using Small-Molecular-Weight Organic Thin Films. *Nature* **2003**, *425*, 158−162.

(18) Cuiffi, J.; Benanti, T.; Nam, W. J.; Fonash, S. Modeling of Bulk And Bilayer Organic Heterojunction Solar Cells. *Appl. Phys. Lett.* **2010**, *96*, No. 143307.

(19) Yu, G.; Gao, J.; Hummelen, J. C.; Wudl, F.; Heeger, A. J. Polymer Photovoltaic Cells-Enhanced Efficiencies via a Network of Internal Donor-Acceptor Heterojunctions. *Science* **1995**, *270*, 1789−1791.

(20) Wang, J. L.; Liu, K. K.; Yan, J.; Wu, Z.; Liu, F.; Xiao, F.; Chang, Z. F.; Wu, H. B.; Cao, Y.; Russell, T. P. Series of Multifluorine Substituted Oligomers for Organic Solar Cells with Efficiency over 9% and Fill Factor of 0.77 by Combination Thermal and Solvent Vapor Annealing. *J. Am. Chem. Soc.* **2016**, *138*, 7687−7697.

(21) Kumar, C. V.; Cabau, L.; Viterisi, A.; Biswas, S.; Sharma, G. D.; Palomares, E. Solvent Annealing Control of Bulk Heterojunction Organic Solar Cells with 6.6% Efficiency Based on a Benzodithiophene Donor Core and Dicyano Acceptor Units. *J. Phys. Chem. C* **2015**, *119*, 20871−20879.

(22) Solanki, A.; Bagui, A.; Long, G. K.; Wu, B.; Salim, T.; Chen, Y. S.; Lam, Y. M.; Sum, T. C. Effectiveness of External Electric Field Treatment of Conjugated Polymers in Bulk-Heterojunction Solar Cells. *ACS Appl. Mater. Interfaces* **2016**, *8*, 32282−32291.

(23) Huang, Y. C.; Chia, H. C.; Chuang, C. M.; Tsao, C. S.; Chen, C. Y.; Su, W. F. Facile Hot Solvent Vapor Annealing for High Performance Polymer Solar Cell Using Spray Process. *Sol. Energy Mater. Sol. Cells* **2013**, *114*, 24−30.

DOI: 10.1021/acsami.8b15140
ACS Appl. Mater. Interfaces 2018, 10, 33399−33406

(24) Na, S. I.; Yu, B. K.; Kim, S. S.; Vak, D.; Kim, T. S.; Yeo, J. S.; Kim, D. Y. Fully Spray-Coated ITO-Free Organic Solar Cells for Low-Cost Power Generation. *Sol. Energy Mater. Sol. Cells* **2010**, *94*, 1333−1337.
(25) Park, S. Y.; Kang, Y. J.; Lee, S.; Kim, D. G.; Kim, J. K.; Kim, J. H.; Kang, J. W. Spray-Coated Organic Solar Cells with Large-Area of 12.25 cm^2. *Sol. Energy Mater. Sol. Cells* **2011**, *95*, 852−855.
(26) Girotto, C.; Moia, D.; Rand, B. P.; Heremans, P. High-Performance Organic Solar Cells with Spray-Coated Hole-Transport and Active Layers. *Adv. Funct. Mater.* **2011**, *21*, 64−72.
(27) Falco, A.; Zaidi, A. M.; Lugli, P.; Abdellah, A. Spray Deposition of Polyethylenimine Thin Films for The Fabrication of Fully-Sprayed Organic Photodiodes. *Org. Electron.* **2015**, *23*, 186−192.
(28) Falco, A.; Cina, L.; Scarpa, G.; Lugli, P.; Abdellah, A. Fully-Sprayed and Flexible Organic Photodiodes with Transparent Carbon Nanotube Electrodes. *ACS Appl. Mater. Interfaces* **2014**, *6*, 10593−10601.
(29) Angmo, D.; Hosel, M.; Krebs, F. C. All Solution Processing of ITO-Free Organic Solar Cell Modules Directly on Barrier Foil. *Sol. Energy Mater. Sol. Cells* **2012**, *107*, 329−336.
(30) Lochner, C. M.; Khan, Y.; Pierre, A.; Arias, A. C. All-Organic Optoelectronic Sensor for Pulse Oximetry. *Nat. Commun.* **2014**, *5*, No. 5745.
(31) Pierre, A.; Deckman, I.; Lechene, P. B.; Arias, A. C. High Detectivity All-Printed Organic Photodiodes. *Adv. Mater.* **2015**, *27*, 6411−6417.
(32) Machui, F.; Lucera, L.; Spyropoulos, G. D.; Cordero, J.; Ali, A. S.; Kubis, P.; Ameri, T.; Voigt, M. M.; Brabec, C. J. Large Area Slot-Die Coated Organic Solar Cells on Flexible Substrates with Non-Halogenated Solution Formulations. *Sol. Energy Mater. Sol. Cells* **2014**, *128*, 441−446.
(33) Kim, Y.; Cook, S.; Tuladhar, S. M.; Choulis, S. A.; Nelson, J.; Durrant, J. R.; Bradley, D. D. C.; Giles, M.; Mcculloch, I.; Ha, C. S.; Ree, M. A Strong Regioregularity Effect in Self-Organizing Conjugated Polymer Films And High-Efficiency Polythiophene: Fullerene Solar Cells. *Nat. Mater.* **2006**, *5*, 197−203.
(34) Kim, Y.; Choulis, S. A.; Nelson, J.; Bradley, D. D. C.; Cook, S.; Durrant, J. R. Device Annealing Effect in Organic Solar Cells with Blends of Regioregular Poly(3-Hexylthiophene) And Soluble Fullerene. *Appl. Phys. Lett.* **2005**, *86*, No. 063502.
(35) Miller, S.; Fanchini, G.; Lin, Y. Y.; Li, C.; Chen, C. W.; Su, W. F.; Chhowalla, M. Investigation of Nanoscale Morphological Changes in Organic Photovoltaics During Solvent Vapor Annealing. *J. Mater. Chem.* **2008**, *18*, 306−312.
(36) Ray, B.; Nair, P. R.; Alam, M. A. Annealing dependent performance of organic bulk-heterojunction solar cells: A theoretical perspective. *Sol. Energy Mater. Sol. Cells* **2011**, *95*, 3287−3294.
(37) Ray, B.; Alam, M. A. Random vs regularized OPV: Limits of Performance Gain of Organic Bulk Heterojunction Solar Cells by Morphology Engineering. *Sol. Energy Mater. Sol. Cells* **2012**, *99*, 204−212.
(38) Chen, D.; Nakahara, A.; Wei, D. G.; Nordlund, D.; Russell, T. P. P3HT/PCBM Bulk Heterojunction Organic Photovoltaics: Correlating Efficiency and Morphology. *Nano Lett.* **2011**, *11*, 561−567.
(39) Benavides, C. M.; Rechberger, S.; Spiecker, E.; Berlinghof, M.; Unruh, T.; Biele, M.; Schmidt, O.; Brabec, C. J.; Tedde, S. F. Improving Spray Coated Organic Photodetectors Performance by Using 1,8-Diiodooctane as Processing Additive. *Org. Electron.* **2018**, *54*, 21−26.
(40) Wang, H.; Xing, S.; Zheng, Y.; Kong, J.; Yu, J.; Taylor, A. D. Three-Phase Morphology Evolution in Sequentially Solution-Processed Polymer Photodetector: Toward Low Dark Current and High Photodetectivity. *ACS Appl. Mater. Interfaces* **2018**, *10*, 3856−3864.
(41) Arca, F.; Tedde, S. F.; Sramek, M.; Rauh, J.; Lugli, P.; Hayden, O. Interface Trap States in Organic Photodiodes. *Sci. Rep.* **2013**, *3*, No. 1324.
(42) Kielar, M.; Dhez, O.; Pecastaings, G.; Curutchet, A.; Hirsch, L. Long-Term Stable Organic Photodetectors with Ultra Low Dark Currents for High Detectivity Applications. *Sci. Rep.* **2016**, *6*, No. 39201.
(43) Leem, D. S.; Lee, K. H.; Kwon, Y. N.; Yun, D. J.; Park, K. B.; Lim, S. J.; Kim, K. S.; Jin, Y. W.; Lee, S. Low Dark Current Inverted Organic Photodetectors Employing Moox: Al Cathode Interlayer. *Org. Electron.* **2015**, *24*, 176−181.
(44) Xiong, S.; Li, L.; Qin, F.; Mao, L.; Luo, B. W.; Jiang, Y. Y.; Li, Z. F.; Huang, J. S.; Zhou, Y. H. Universal Strategy To Reduce Noise Current for Sensitive Organic Photodetectors. *ACS Appl. Mater. Interfaces* **2017**, *9*, 9176−9183.
(45) Agostinelli, T.; Campoy-Quiles, M.; Blakesley, J. C.; Speller, R.; Bradley, D. D. C.; Nelson, J. A Polymer/Fullerene Based Photodetector with Extremely Low Dark Current for X-Ray Medical Imaging Applications. *Appl. Phys. Lett.* **2008**, *93*, No. 203305.
(46) Ng, T. N.; Wong, W. S.; Chabinyc, M. L.; Sambandan, S.; Street, R. A. Flexible Image Sensor Array with Bulk Heterojunction Organic Photodiode. *Appl. Phys. Lett.* **2008**, *92*, No. 213303.
(47) Armin, A.; Hambsch, M.; Kim, I. K.; Burn, P. L.; Meredith, P.; Namdas, E. B. Thick Junction Broadband Organic Photodiodes. *Laser Photonics Rev.* **2014**, *8*, 924−932.
(48) Armin, A.; Jansen-van Vuuren, R. D.; Kopidakis, N.; Burn, P. L.; Meredith, P. Narrowband Light Detection via Internal Quantum Efficiency Manipulation of Organic Photodiodes. *Nat. Commun.* **2015**, *6*, No. 6343.
(49) Baierl, D.; Pancheri, L.; Schmidt, M.; Stoppa, D.; Dalla Betta, G. F.; Scarpa, G.; Lugli, P. A Hybrid CMOS-imager with a Solution-Processable Polymer as Photoactive Layer. *Nat. Commun.* **2012**, *3*, No. 1175.
(50) Zeng, L. C.; Tang, C. W.; Chen, S. H. Effects of Active Layer Thickness And Thermal Annealing on Polythiophene: Fullerene Bulk Heterojunction Photovoltaic Devices. *Appl. Phys. Lett.* **2010**, *97*, No. 053305.
(51) Zhao, Y.; Duan, L. P.; Liu, J. T.; Xu, Q.; Ni, Z. H. Optimisation of Thermal Annealing Parameters for Different Thickness of Active Layers Based on Polymer/Fullerene Bulk Heterojunction Solar Cells. *Mater. Res. Innovations* **2013**, *17*, S152−S155.
(52) Kan, B.; Zhang, Q.; Li, M. M.; Wan, X. J.; Ni, W.; Long, G. K.; Wang, Y. C.; Yang, X.; Feng, H. R.; Chen, Y. S. Solution-Processed Organic Solar Cells Based on Dialkylthiol-Substituted Benzodithiophene Unit with Efficiency near 10%. *J. Am. Chem. Soc.* **2014**, *136*, 15529−15532.
(53) Lin, M. C.; Huang, Y. C.; Yen, C. T.; Tsao, C. S.; Lin, M. C. The Effect of Hole Transport Layer on The Thermal Stability of Inverted Polymer Solar Cells. *Polym. Degrad. Stab.* **2016**, *134*, 245−250.
(54) Huang, Y. C.; Hsu, F. H.; Cha, H. C.; Chuang, C. M.; Tsao, C. S.; Chen, C. Y. High-Performance ITO-Free Spray-Processed Polymer Solar Cells with Incorporating Ink-Jet Printed Grid. *Org. Electron.* **2013**, *14*, 2809−2817.
(55) Mihailetchi, V. D.; Xie, H. X.; de Boer, B.; Koster, L. J. A.; Blom, P. W. M. Charge Transport And Photocurrent Generation in Poly(3-Hexylthiophene): Methanofullerene Bulk-Heterojunction Solar Cells. *Adv. Funct. Mater.* **2006**, *16*, 699−708.
(56) Erb, T.; Zhokhavets, U.; Gobsch, G.; Raleva, S.; Stuhn, B.; Schilinsky, P.; Waldauf, C.; Brabec, C. J. Correlation between Structural And Optical Properties of Composite Polymer/Fullerene Films for Organic Solar Cells. *Adv. Funct. Mater.* **2005**, *15*, 1193−1196.
(57) Rujisamphan, N.; Deng, F.; Murray, R. E.; Ni, C. Y.; Shah, S. I. Focused Ion Beam Assisted Investigations of Al Interface in Polythiophene:Fullerene Solar Cells. *Sol. Energy Mater. Sol. Cells* **2013**, *109*, 56−62.
(58) Perrier, G.; de Bettignies, R.; Berson, S.; Lemaitre, N.; Guillerez, S. Impedance Spectrometry of Optimized Standard and Inverted P3HT-PCBM Organic Solar Cells. *Sol. Energy Mater. Sol. Cells* **2012**, *101*, 210−216.

DOI: 10.1021/acsami.8b15140
ACS Appl. Mater. Interfaces 2018, 10, 33399−33406

(59) Barsoukov, E.; Macdonald, J. R. *Impedance Spectroscopy: Theory, Experiment, and Applications*, 2nd ed.; John Wiley & Sons, Inc.: NJ, 2005.
(60) Liao, H.-C.; Tsao, C.-S.; Lin, T.-H.; Chuang, C.-M.; Chen, C.-Y.; Jeng, U. S.; Su, C.-H.; Chen, Y.-F.; Su, W.-F. Quantitative Nanoorganized Structural Evolution for A High Efficiency Bulk Heterojunction Polymer Solar Cell. *J. Am. Chem. Soc.* **2011**, *133*, 13064−13073.
(61) Liao, H.-C.; Tsao, C.-S.; Lin, T.-H.; Jao, M.-H.; Chuang, C.-M.; Chang, S.-Y.; Huang, Y.-C.; Shao, Y.-T.; Chen, C.-Y.; Su, C.-J.; Jeng, U. S.; Chen, Y.-F.; Su, W.-F. Nanoparticle-Tuned Self-Organization of a Bulk Heterojunction Hybrid Solar Cell with Enhanced Performance. *ACS Nano* **2012**, *6*, 1657−1666.
(62) Huang, Y.-C.; Tsao, C.-S.; Cha, H.-C.; Chuang, C.-M.; Su, C.-J.; Jeng, U. S.; Chen, C.-Y. Correlation between Hierarchical Structure and Processing Control of Large-area Spray-coated Polymer Solar Cells toward High Performance. *Sci. Rep.* **2016**, *6*, No. 20062.

DOI: 10.1021/acsami.8b15140
ACS Appl. Mater. Interfaces 2018, 10, 33399−33406